Photocatalytic reduction of CO_2 by graphitic carbon nitride polymers derived from urea and barbituric acid

Jiani Qin, Sibo Wang, He Ren, Yidong Hou, Xinchen Wang*

State Key Laboratory of Photocatalysis on Energy and Environment, College of Chemistry, Fuzhou University, Fuzhou 350002, PR China

ABSTRACT

Conjugated carbon nitride nanosheets modified with barbituric acid (BA) were synthesized by a facile one-pot chemical condensation of urea. The obtained BA-modified carbon nitride samples were termed as CNU-BA$_X$ and were fully characterized by XRD, FTIR, XPS, NMR, EPR, FESEM, TEM, DRS, PL, BET and photocurrent measurements. The performance of the developed carbon nitride based semiconductors was investigated by applying them as polymeric photocatalysts for the reduction of CO_2 under visible light illumination. Results revealed that the copolymerization of urea with BA co-monomer strongly alternated the physical and chemical properties of carbon nitride polymer by improving optical absorption and creating surface molecular heterojunction that promoted charge separation, and consequently the enhanced photocatalytic performance was achieved. Various reaction parameters were investigated and optimized for the reaction system, and we found that under the optimal reaction condition, the best sample (CNU-BA$_{0.03}$) could effectively photocatalyze the CO_2-to-CO conversion reaction with 15-fold-enhanced catalytic activity, compared to the non-modified sample derived from urea (named as CNU). Other typical comonomers were also selected to polymerize with urea to study the beneficial effect of copolymerization on the development of efficient carbon nitride based nanostructures for CO_2 photoreduction.

© 2015 Elsevier B.V. All rights reserved.

1. Introduction

Since the pioneer work by Inoue et al. [1], semiconductor-mediated photocatalytic CO_2 conversion driven by solar energy has attracted much attention as it promises solar technology in solving global energy and environmental problems [2–5]. TiO_2 based semiconductors have been recognized as the most widely-investigated photocatalysts during the past 3 decades for solar to chemical energy conversion via artificial photosynthetic reactions, like water photosplitting [6–8] and CO_2 photofixation [9–12]. Various semiconductors such as CdS [13], ZrO_2 [14], Ga_2O_3 [15], $InTaO_4$ [16,17], $ZnGa_2O_4$ [18] and $ZnGe_2O_4$ [19] have also advanced as photocatalysts for the photochemical reduction of CO_2. However, most of these photocatalysts are either UV-light responsive or made of expensive/scare metal species that limits their long term and large scale applications. Therefore, it is imperative to develop easy-accessible, metal-free, high-stable and visible light responsive materials to accomplish the crucial mission of solar-driven CO_2 fixations for sustainable production of energized chemicals and fuels.

Graphitic carbon nitride (g-C_3N_4), an emerging polymeric semiconductor, has been introduced as a metal-free, polymeric photocatalyst for water splitting [20–24] and organic synthesis [25–27], as inspired by the report in 2009 for photocatalytic hydrogen and oxygen evolution under visible light irradiation [28]. Recently, the photocatalytic application of g-C_3N_4 has been extended for the reduction of CO_2 by several groups [29–37], because of its unique semiconductor and surface characteristics that allow the creation of charge carriers for the reduction of the pre-adsorbed/activated CO_2 molecules by the surface basic sites on nitrogen-rich carbon nitride frameworks with tunable texture and surface functions. However, the catalytic efficiency of these developed CO_2 conversion systems is moderate towards the practical applications, even decorated with additional promotional components such as cobalt based cocatalysts [29,32]. The modification on the intrinsic properties of g-C_3N_4 together with its surface kinetic controls is desired to enhance the photocatalytic performance of g-C_3N_4 for CO_2 photoreduction. Especially, the modification tools for tuning the electronic structure, texture and surface structure of g-C_3N_4 has already been established for photocatalytic hydrogen evolution [38–42] and organic functional transformation reactions [25,26]. It is therefore desirable to

translate these modification schemes and knowledge to promote CO_2 reduction reactions by g-C_3N_4, which could further couple with water splitting and organosynthesis to achieve artificial photosynthesis.

In our previous works, we have demonstrated that, through a copolymerization strategy using dicyandiamide (DCDA) and conjugated organic monomers, the catalytic activity of the obtained g-C_3N_4 based photocatalysts can be significantly improved for their applications in water photosplitting [43–45] and organic photosynthesis [46]. Such a copolymerization not only enhanced the optical absorption of g-C_3N_4 as a result of pi-system extension, but also created surface dissimilar molecular junctions that promoted charge collection and separation on the polymer surface for photoredox catalysis. In addition, we have already demonstrated that the nanostructure engineering of g-C_3N_4 can be easily achieved by using the self-polymerization of urea to obtain carbon nitride nanosheets with reduced charge diffusion of 3–5 nm that significantly enhanced surface area of the materials and accelerate charge separation [47].

In this paper, the copolymerization and nanostructure engineering strategy were combined to modify the optical, surface and nanostructural properties of g-C_3N_4 semiconductors, with hope of creating synergistic effect for efficient CO_2 reduction with photon. Indeed, it was found that the catalytic performance of g-C_3N_4 for the photochemical conversion of CO_2 can be remarkably promoted by the copolymerization and nanostructure engineering strategy using barbituric acid as the co-monomer to polymerize with urea precursor. After incorporating the unique organic function of BA into the framework of carbon nitride nanosheets, the BA-modified samples exhibited improved visible light absorption, suppressed electron-hole recombination rates and promoted charge transports, which endows them as favorable candidates for heterogeneous photocatalytic CO_2 conversion reactions. The synthesized CNU-BA$_X$ samples were systematically characterized and the reaction parameters were investigated and optimized. Under the optimal reaction conditions, BA-CNU$_{0.03}$ exhibited 15-fold-enhanced catalytic activity for the CO_2-to-CO transformation reaction compared with the parental CNU sample. The stability of the BA-modified carbon nitride in the photocatalytic CO_2 reduction system was solidly confirmed during a repeated operation of the reactions. The generalization of copolymerization and nanostructure engineering strategy to remarkably enhance the catalytic performance of carbon nitride for CO_2 photoreduction was further validated by using other typical comonomers (e.g., 2-aminothiophene-3-carbonitrile, ATCN; 2-aminobenzonitrile, ABN; diaminomaleonitrile, DAMN) to copolymerize with urea.

2. Experimental

2.1. Chemicals

All the chemical reagents for the photocatalytic reactions were used without further purification. Urea, barbituric acid (BA), 2,2′-bipyridine (bpy), CoCl$_2$ were purchased from Sigma. The organic solvents, including acetonitrile (MeCN), N,N-dimethylformamide (DMF), trichloromethane (TCM) and tetrahydrofuran (THF) were purchased from China Sinopharm Chemical reagent Co., Ltd. Carbon dioxide gas, supplied by Fuzhou Lianzhong Industrial Gases Co., Ltd is super grade purity (99.999%). The ^{13}CO (98% enriched) was purchased from Hess chemical gas center in Beijing.

2.2. Synthesis of photocatalysts

CNU sample was prepared by directly heating urea (10 g) at 550 °C for 2 h with a ramping rate of 5.0 °C min^{-1} in air.

To synthesize BA modified CNU samples, urea (10 g) and different amounts of BA were dissolved in 10 mL deionized water with stirring at 100 °C to remove water, then the obtained solids were calcined at 550 °C for 2 h with the same heating rate. The harvested samples were denoted as CNU-BA$_X$, where x (0.01, 0.03, 0.05, 0.1, 0.3) was the weight-in amount of BA. Other modified CNU samples were synthesized through the similar method. The obtained samples were named as CNU-ABN$_{0.03}$ (2-aminobenzonitrile), CNU-ATCN$_{0.03}$ (2-aminothiophene-3-carbonitrile) and CNU-DAMN$_{0.03}$ (diaminomaleonitrile), accordingly.

2.3. Characterization

A Bruker D8 Advance diffractometer with Cu Kα1 radiation were employed to conduct X-ray diffraction (XRD) measurements. Fourier transformed infrared (FTIR) spectra were obtained on a Nicolet Magna 670 fourier transform infrared spectrometer. X-ray photoelectron spectroscopy (XPS) measurements were conducted on Thermo ESCALAB250 instrument with a monochromatized Al Ka line source (200 W). The solid-state ^{13}C NMR experiments were performed on a Bruker Advance III 500 spectrometer. The electron paramagnetic resonance (EPR) measurements were carried out on a Bruker model A300 spectrometer. Morphologies of the samples were characterized by Hitachi New Generation SU8010 field emission scanning electron microscope (FESEM). Transmission electron microscopy (TEM) was performed on a JEOL model JEM 2010 EX instrument. The UV–vis diffuse reflectance spectra (DRS) of the samples were conducted on a Varian Cary 500 Scan UV–vis spectrophotometer with barium sulfate as the reference. Photoluminescence (PL) spectra were collected on an Edinburgh FI/FSTCSPC 920 spectrophotometer. The photocurrent measurements were performed on a CHI electrochemical system. N$_2$ adsorption-desorption and CO_2 adsorption isotherms were measured on Micromeritics ASAP2020 equipment.

An Agilent 7820A gas chromatography, equipped with a thermal conductivity detector (TCD) and a TD-01 packed column, was employed to analyze the produced gases. The ^{13}CO generated from the $^{13}CO_2$ isotopic experiment was analyzed on a HP 5973 gas chromatography-mass spectrometry (GC–MS).

2.4. Photocatalytic test

A 300 W Xe lamp with a 420 nm cut-off filter was utilized as the light source for the typical photocatalytic reactions. In brief, 30 mg catalyst, 1 μmol CoCl$_2$, 15 mg 2,2-bipyridine, 1 mL triethanolamine (TEOA) and 5 mL solvent were added to the Schlenk flask reactor (80 mL in capacity). After 3 times vacuum degassing and backfilling the reactor with pure CO_2, the reaction system was finally filled with CO_2 (1 atm). In the whole reaction process, the reaction system was energetically stirred and the reaction temperature was maintained at 30 °C with cooling water system. After the photocatalytic reactions, the produced gases were analyzed by a gas chromatography. The isotopic experiment was carried out by using $^{13}CO_2$ as the reactant under otherwise identical photocatalytic reaction conditions, and a gas chromatography-mass spectrometry (GC–MS) was utilized to analyze the generated ^{13}CO.

3. Results and discussion

3.1. Characterization of the samples

The modified CNU-BA$_X$ samples were characterized by XRD measurement. As shown in Fig. 1a, all the samples present similar characteristic XRD peaks as those of the CNU sample. It is clear that with increasing amount of BA, the peaks at 13.0° assigned to the lattice planes parallel to the c-axis are weakened
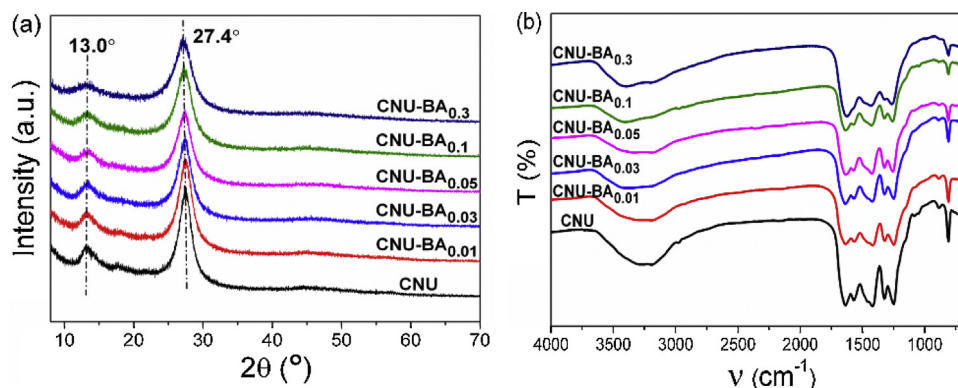
Fig. 1. (a) XRD patterns and (b) FTIR spectra of CNU and CNU–BA$_X$ samples.

and broadened, and the intensity of the graphite-like interlayer (0 0 2) peak at 27.4° obviously decreases. The results could originate from the disturbance of graphitic structure by inserting BA motifs in the layered structure. The FTIR spectra (Fig. 1b) exhibit all the characteristic stretch modes of aromatic CN heterocycles at 1200–1600 cm^{-1} together with the breathing mode of the heptazine units (810 cm^{-1}). The broad peaks between 3000 cm^{-1} and 3600 cm^{-1} contributed by the N—H stretching, confirming the existence of NH and/or NH$_2$ groups on the surface.

XPS measurements were conducted to get insights into the chemical composition and chemical status of the elements in the synthesized samples. The survey spectra reveal that only C and N elements exist in both CNU and CNU-BA$_{0.03}$ samples, and the little O element was attributed to the absorbed H$_2$O and CO$_2$ on the surface of the samples (Fig. S1). Two peaks were observed in the C 1s high-resolution XPS spectrum (Fig. 2a), the main peak at 287.9 eV was assigned to N—C=N coordination, and the other one at 284.6 eV was attributed to the sp^2 C—C bonds, originating from the carbon-containing contamination [48]. In the high-resolution XPS spectrum of N 1s (Fig. 2b), the detected four peaks at 398.4 eV, 399.6 eV, 400.7 eV and 404.2 eV were correspondingly assigned to the sp^2 C—N=C bonds, the tertiary nitrogen N—(C)3 groups, the amino groups C—N—H and the charging effects or positive charge localization in the heterocycles [48]. The results of FTIR and XPS characterizations demonstrated the well preserve of the structure and core chemical skeleton of CNU, as well as the successful construction of tri-s-triazine based covalent networks through the copolymerization strategy.

Fig. 3a shows the solid-state ^{13}C NMR spectra of the CNU and CNU-BA samples. A new weak peak appeared at $\delta \approx 94$ ppm was detected for CNU-BA sample as compared to non-modified CNU sample. The finding indicates that new carbon was incorporated

into the structure but the heptazinc-based structure of CNU was not altered [49]. Moreover, the electron paramagnetic resonance (EPR) characterizations were also conducted to explore the electronic band structure of the prepared carbon nitride materials. As shown in Fig. 3b, at room temperature, all the samples exhibit one single Lorentzian lines centered at 3515 G with a g-value of 2.0034. This EPR signal is gradually enhanced as the increase in incorporated degree with BA monomer. We attribute this to the unpaired electrons of the carbon atoms in the aromatic rings, within π-bonded nanosized clusters on the surface of the semiconductors [50]. Under visible light irradiation, the EPR signals for both CNU and CNU-BA$_{0.03}$ samples were further increased (Fig. 3c), suggesting the efficient generation of photochemical radical pairs on the samples, which is virtually consistent with our previous results [43,51].

To study the surface morphology and texture of CNU-BA$_{0.03}$ sample, field emission scanning electron microscopy (FESEM) and transmission electron microscopy (TEM) characterizations were performed. The typical FESEM images of CNU and CNU-BA$_{0.03}$ samples are shown in Fig. 4a and b, respectively. For the CNU sample, dense and stacked particles and sheets are observed. While in the case of CNU-BA$_{0.03}$, it exhibits lamellar nanostructured architectures with many irregular holes, which is significantly distinctive from its pristine sample obtained only using urea as the precursor. The TEM measurements further revealed the thin, silk-like nanosized architecture of CNU-BA$_{0.03}$ (Fig. 4d), which is inherited from the defoliation of the big sheets of the pristine CUN sample (Fig. 4c).

Another obvious change of the modified CNU-BA$_X$ samples are their macroscopic deeper orange color quite different from the pale yellow for the CNU sample, which is also a proof of the modification of aromatic π-conjugated system in nanosheets matrix, illustrating the success in the improved visible-light harvesting by
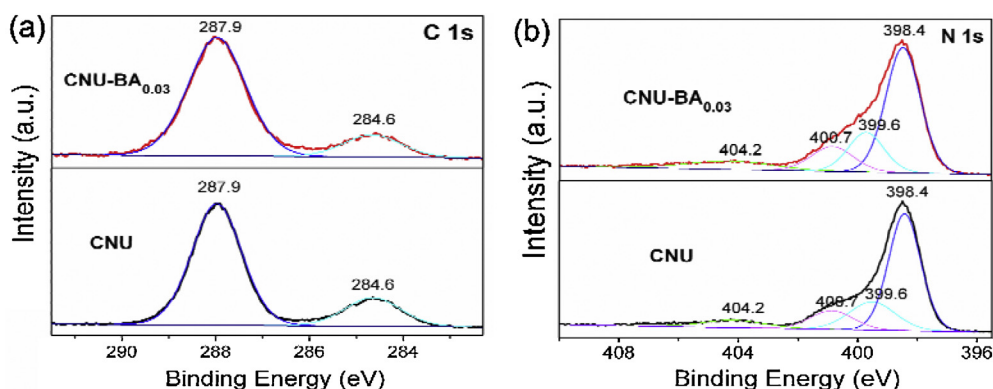

Fig. 2. (a) C 1s and (b) N 1s high-resolution XPS spectra of the CNU–BA$_{0.03}$ and CNU samples.
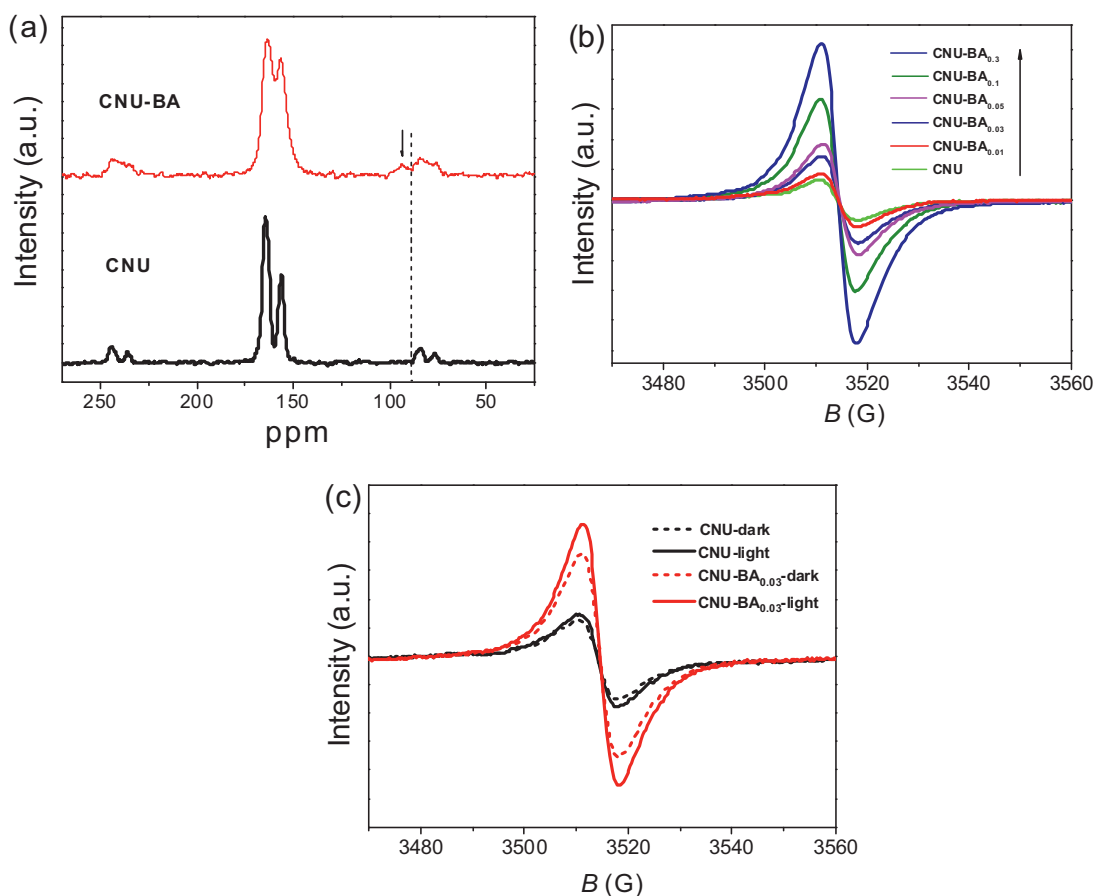
Fig. 3. (a) Solid-state ^{13}C NMR spectra and EPR spectra (b) in the dark; (c) under visible light ($\lambda \geqq 420$ nm) for CNU and CNU–BA samples.

chemical and nanostructure engineering. The DRS spectra provide more detailed information about the color changes of the samples. As displayed in Fig. 5, remarkable red-shifts of the optical edges of BA-modified CNU samples (440–520 nm) are achieved compared with the pristine CNU sample (425 nm). The observations disclose that the enhanced light adsorption ability is actually attributed to the narrowing of the band gap.

The photoluminescence (PL) spectra (Fig. 6a) demonstrate that the PL peaks of all the CNU-BA$_X$ samples are gradually shifted toward longer wavelength as the modified content of BA is increased, together with the significant diminishment in intensity, which indicated that the suppressed electron-hole recombination rates mainly results from the extension of the π-conjugation. Furthermore, the photocurrent (I_{ph}) measurements of the samples shows the notable enhancement in the I_{ph} of CNU-BA$_{0.03}$ over CNU (Fig. 6b), reflecting the enhanced efficiency of the charge transfer process [52]. The improved optical absorption, the lowered electron-hole recombination rates, and the promoted charge transports of the CNU-BA$_X$ samples render them as favorable candidates for heterogeneous photocatalytic CO_2 reduction reactions.
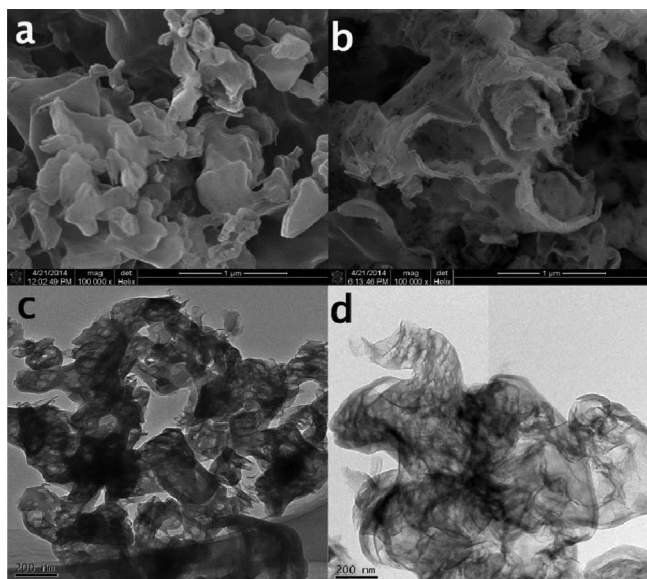

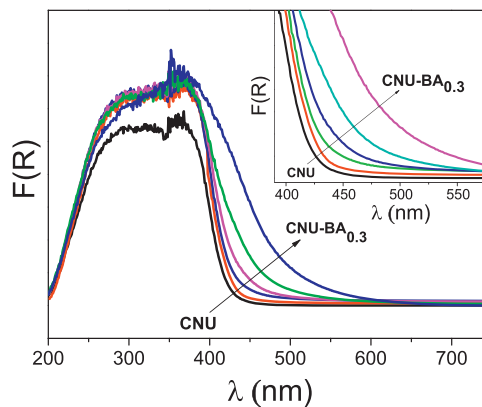**Fig. 4.** SEM and TEM images of CNU (a, c) and CNU–BA$_{0.03}$ (b, d).

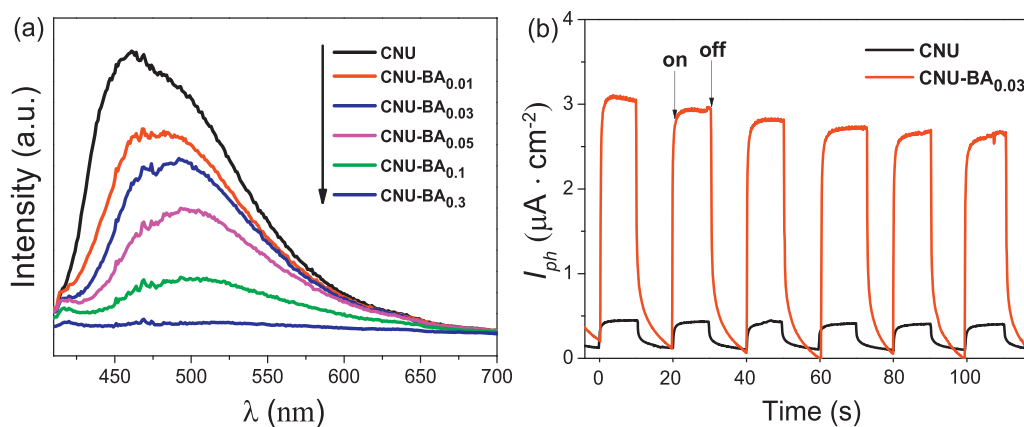**Fig. 5.** UV–vis DRS spectra of the samples.

Fig. 6. (a) The photoluminescence spectrum of the CNU and CNU–BA$_X$ samples under 400 nm excitation, (b) Photoelectrochemical properties of the CNU and CNU–BA$_{0.03}$ samples at Ag/AgCl in a 0.2 M Na$_2$SO$_4$ aqueous solution (pH 6.8). Periodic on/off photocurrent response under visible light irradiation ($\lambda \geqq 420$ nm).
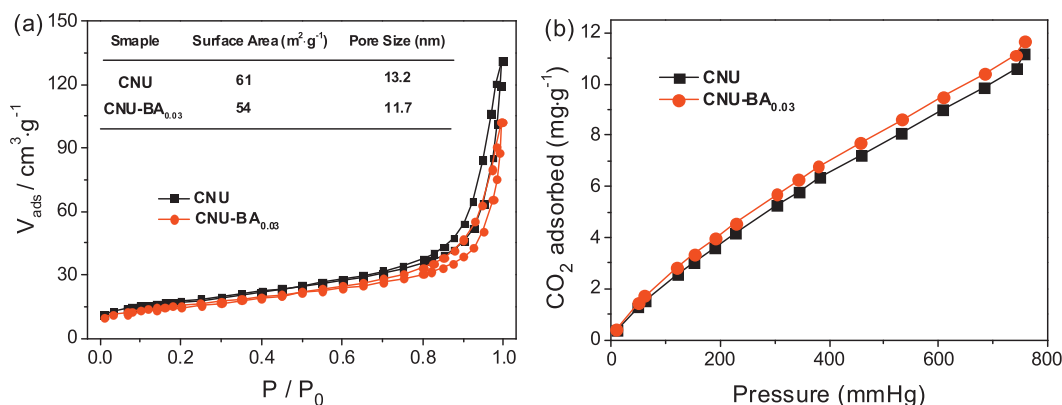

Fig. 7. (a) N$_2$ adsorption–desorption isotherms (77 K) and (b) CO$_2$ adsorption isotherms (273 K) for CNU and CNU–BA$_{0.03}$ samples.

N$_2$ adsorption-desorption and CO$_2$ adsorption isotherms were carried out to analyze the surface properties of the samples (Fig. 7a and b). The N$_2$ adsorption–desorption isotherms for both CNU and CNU-BA$_{0.03}$ samples, according to the IUPAC classification, exhibit a type IV behavior with an H1 type hysteresis loop, demonstrating the mesoporous characteristic the materials [53]. The BET surface area is *ca.* 61 m^2 g^{-1} for CNU and 54 m^2 g^{-1} for CNU-BA$_{0.03}$. Interestingly, the CNU-BA$_{0.03}$ shows improved adsorption capability toward CO$_2$ compared to CNU (Fig. 7b), that is, the introduction of BA monomer into the carbon nitride precursor slightly diminishes the surface area, but increases the active molecular docking sites of CO$_2$ adsorption, which is favorable for CO$_2$ photofixation reaction.

3.2. Photocatalytic property

With the prepared CNU-BA$_{0.03}$ sample as the photocatalyst, we performed the visible-light CO$_2$ reduction reaction in the mixture of water and acetonitrile (MeCN) containing Co(bpy)$_3{}^{2+}$ and TEOA to act as a cocatalyst and a sacrificial electron donor, correspondingly. Fig. 8 shows the productions of CO and H$_2$ as a function of reaction time. In the four-hour-reaction, 56.3 μmol CO and 12.5 μmol H$_2$ were generated from the reaction system, establishing a turnover number (TON) of more than 68 with respect to Co^{2+}, revealing the catalytic feature of the reaction. This catalytic efficiency is much higher than the previously reported data [29,54].

Results of the controlled experiments (Table S1) reflected that the CO$_2$ photoreduction reaction was completely terminated with any absence of components in chemical system (e.g., CNU-BA$_{0.03}$, Co(bpy)$_3{}^{2+}$, TEOA, CO$_2$). No detection of CO or H$_2$ in dark reveals
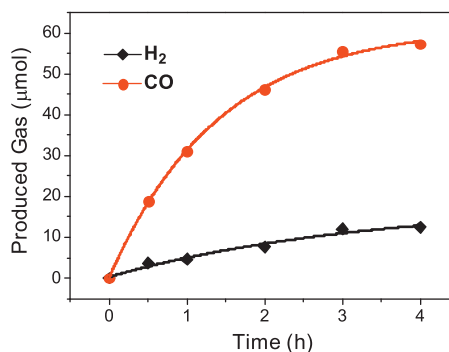

Fig. 8. Time-production plot of the CO and H$_2$ generated form the photocatalytic CO$_2$ reduction system with CNU–BA$_{0.03}$ under visible light illumination.

that the reaction proceeds photocatalytially. To get insights into the carbon source of the CO generated, ^{13}C-labelled isotropic experiment was carried out. As shown in Fig. 9, the peak in the gas chromatogram (RT = 3.69) with the *m/z* value of 29 is a clear indicator of ^{29}(CO), saying that the generated CO was originated from the CO$_2$ reactant, not the other substance in the catalytic system. It was also revealed by LC–MS analysis that the alcohol group of the sacrificial TEOA is oxidized to an aldehyde (Fig. S4), which is a well known reaction in organic chemistry from N-oxides. Various reaction parameters including the concentration of Co^{2+} (Fig. S2), reaction temperature (Fig. S3), and reaction medium (Table S2) were also carefully investigated and optimized for chemical system to efficiently manipulate the CO$_2$ conversion catalysis.
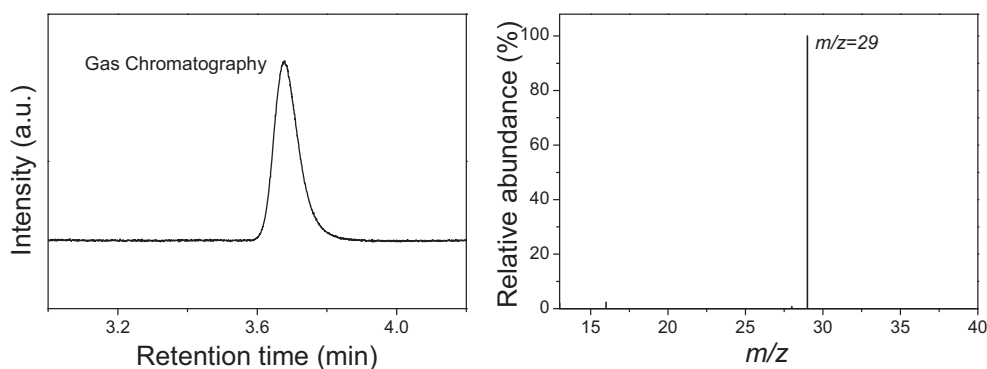
Fig. 9. Gas chromatography and mass spectra ($m/z = 29$) analyses of the carbon source of the generated CO in the photochemical reduction of $^{13}CO_2$.
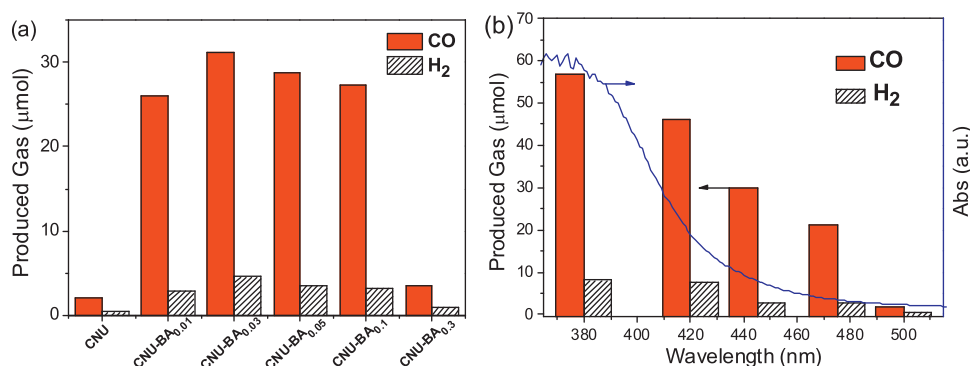

Fig. 10. (a) Effects of the mass of BA incorporated to CNU on the yields of CO and H_2 from the CO_2 photoreduction system. (b) The dependence of the wavelength of incident light on the evolution of CO and H_2 from the photocatalytic reaction of CO_2 reduction system.

Series of BA-modified carbon nitride catalysts were then prepared by changing of the mass of BA co-monomer and examined their catalytic performance for the photocatalytic CO_2-to-CO conversion reaction. As shown in Fig. 10a, the parental CNU catalyst only shows a very low activity for the CO_2 reduction reaction. However, after copolymerized with BA, all the synthesized CNU-BA$_X$ samples exhibit remarkably enhanced catalytic activity for the photosplitting of CO_2 to CO, and particularly, the CNU-BA$_{0.03}$ sample presents the best catalytic performance with a CO evolution rate of 31.1 μmol h^{-1}, which is 15 times higher than that of CNU. The promotion in the catalytic efficiency of CNU-BA$_X$ is mainly originated from the improved light harvesting ability by copolymerization. It is also revealed that when excessive BA was doped, a negative effect emerged as indicated by CNU-BA$_{0.3}$, which is ascribed to destruction of the conjugated structures of carbon nitride by introducing too much dopant. The results point out that the degree of polymerization must be appropriately controlled for promoting the photoredox activity of carbon nitride.

The wavelength-dependent generation of the products catalyzed by CNU-BA$_{0.03}$ revealed that the trend of the yield of CO/H_2 corresponds well to the optical absorption of CNU-BA$_{0.03}$ (Fig. 10b). Clearly, the productions of CO and H_2 diminish with the increase in incident wavelength, but the photocatalytic performance is still observed at 500 nm despite the low efficiency, suggesting the harvested visible photons are the main driving force of the photocatalytic reaction.

To test the stability of the modified CNU-BA$_{0.03}$ catalyst, after photocatalytic reactions, the catalyst was filtrated, recovered and then reused in a fresh reaction mixture for five cyclic operations. As displayed in Fig. 11, there is no evident decrease in the productions of the products for the CO_2 conversion system in the stability test. Based on the total evolution of products, a TON of ca. 170 was achieved with respect to the cobalt species.
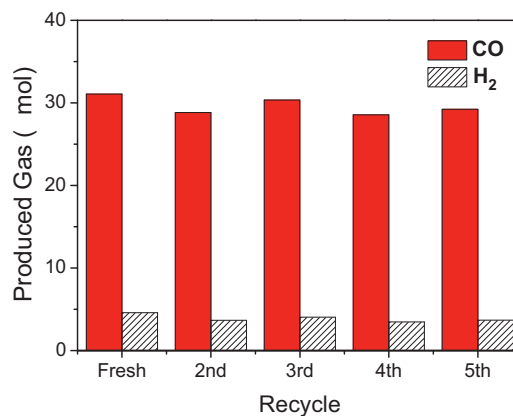

Fig. 11. Stability study of the catalytic evolution of CO and H_2 over the CNU–BA$_{0.03}$ photocatalyst.

Furthermore, after photocatalytic reactions, the used CNU-BA$_{0.03}$ sample was further subjected to structural characterizations by XRD, FTIR and XPS. As displayed in Fig. 12, no noticeable alternations in the crystal, chemical, and surface structure are observed, which confirms the high stability of BA-modified CUN photocatalyst in the current CO_2 reduction system.

To further demonstrate the universality of this copolymerization and nanostructure engineering strategy to modify carbon nitride semiconductors with the purpose of improving catalytic performance for the photochemical reduction of CO_2, some other typical comonomers (e.g., 2-aminothiophene-3-carbonitrile, ATCN; 2-aminobenzonitrile, ABN; diaminomaleonitrile, DAMN) were employed as the comonomers to conjugate with urea. As shown in Fig. 13, all the samples modified by the selected
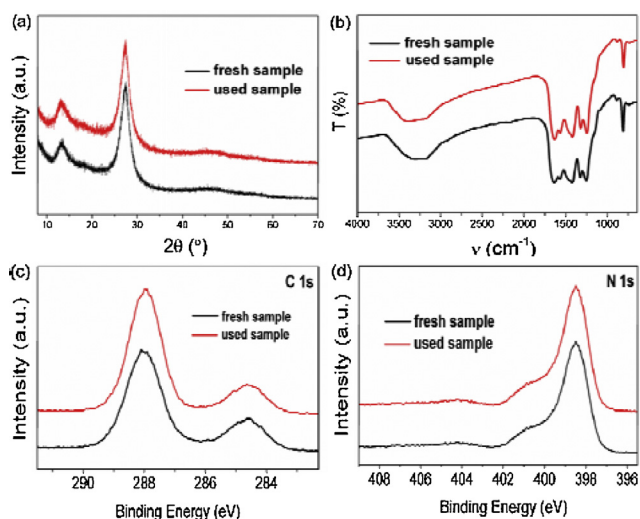
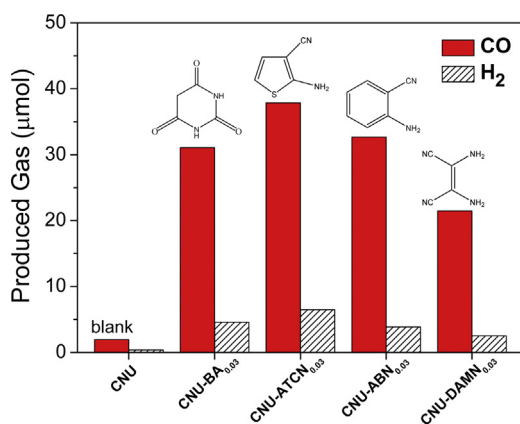**Fig. 12.** Powder XRD (a), FT–IR (b), XPS C1s (c) and N1s (d) patterns for fresh sample and used sample.

Fig. 13. The yields of CO and H_2 over CNU and different co-monomers modified CNU photocatalysts under visible light.

organics also show very good performance, by combining the unique chemical functions of the organic comonomers with carbon nitride precursor. Particularly, the ATCN-doped sample CNU-ATCN$_{0.03}$ shows the highest catalytic activity for the targeted reaction with a CO formation of 37.9 μmol, which is 19-fold-enhanced as compared with the blank sample CNU. These observations clearly indicate that through copolymerization with proper organic comonomers, the catalytic activity of pristine carbon nitride semiconductor for CO_2 reduction can be remarkably improved, promising the ample choice of organic protocols to modulate carbon nitride photocatalysis for CO_2 reduction.

4. Conclusion

With a copolymerization and nanostructure engineering strategy, the optical, surface and nanostructural properties of g-C_3N_4 semiconductor were intentionally modified by incorporating the unique organic function of BA into the framework of carbon nitride nanosheets. The modified samples showed improved optical absorption, reduced electron-hole recombination rates, and enhanced charge transfers, which endows them as efficient heterogeneous photocatalysts for the deoxygenative reduction of CO_2 to CO with visible light. Under the optimal reaction conditions, the best sample (BA-CNU$_{0.03}$) exhibited 15-fold-enhanced catalytic activity for the CO_2-to-CO conversion reaction compared to the parental CNU sample. The stability of the BA-modified carbon nitride in the photocatalytic CO_2 reduction system was confirmed during the repeated operation of the photocatalytic reactions. The universal of copolymerization to remarkably enhance the catalytic performance of carbon nitride for CO_2 photoreduction was further identified by extending other typical comonomers to conjugate with urea. We believe that the present work would bring new opportunities to promote the catalytic performance of carbon nitride photocatalysts in CO_2 photofixations.

Appendix A. Supplementary data

Supplementary data associated with this article can be found, in the online version, at http://dx.doi.org/10.1016/j.apcatb.2015.05.005.

References

[1] T. Inoue, A. Fujishima, S. Konishi, K. Honda, Nature 277 (1979) 637–638.
[2] M. Calvin, Acc. Chem. Res. 11 (1978) 369–374.
[3] M. Aresta, A. Dibenedetto, A. Angelini, Chem. Rev. 114 (2013) 1709–1742.
[4] W.C. Chueh, C. Falter, M. Abbott, D. Scipio, P. Furler, S.M. Haile, A. Steinfeld, Science 330 (2010) 1797–1801.
[5] H. Tong, S.X. Ouyang, Y.P. Bi, N. Umezawa, M. Oshikiri, J.H. Ye, Adv. Mater. 24 (2012) 229–251.
[6] S.U.M. Khan, M. Al-Shahry, W.B. Ingler, Science 297 (2002) 2243–2245.
[7] A. Galińska, J. Walendziewski, Energy Fuels 19 (2005) 1143–1147.
[8] Y. Ma, X. Wang, Y. Jia, X. Chen, H. Han, C. Li, Chem. Rev. 114 (2014) 9987–10043.
[9] J. Yu, J. Low, W. Xiao, P. Zhou, M. Jaroniec, J. Am. Chem. Soc. 136 (2014) 8839–8842.
[10] A. Dhakshinamoorthy, S. Navalon, A. Corma, H. Garcia, Energy Environ. Sci. 5 (2012) 9217–9233.
[11] K. Kočí, L. Obalová, L. Matějová, D. Plachá, Z. Lacný, J. Jirkovský, O. Šolcová, Appl. Catal. B 89 (2009) 494–502.
[12] M. Tahir, N.S. Amin, Appl. Catal. B 142–143 (2013) 512–522.
[13] B.-J. Liu, T. Torimoto, H. Yoneyama, J. Photochem. Photobiol. A 113 (1998) 93–97.
[14] Y. Kohno, T. Tanaka, T. Funabiki, S. Yoshida, Phys. Chem. Chem. Phys. 2 (2000) 5302–5307.
[15] H. Park, J.H. Choi, K.M. Choi, D.K. Lee, J.K. Kang, J. Mater. Chem. 22 (2012) 5304–5307.
[16] C.-W. Tsai, H.M. Chen, R.-S. Liu, K. Asakura, T.-S. Chan, J. Phys. Chem. C 115 (2011) 10180–10186.
[17] P.-Y. Liou, S.-C. Chen, J.C.S. Wu, D. Liu, S. Mackintosh, M. Maroto-Valer, R. Linforth, Energy Environ. Sci. 4 (2011) 1487–1494.
[18] S.C. Yan, S.X. Ouyang, J. Gao, M. Yang, J.Y. Feng, X.X. Fan, L.J. Wan, Z.S. Li, J.H. Ye, Y. Zhou, Z.G. Zou, Angew. Chem. Int. Ed. 49 (2010) 6400–6404.
[19] Q. Liu, Y. Zhou, J. Kou, X. Chen, Z. Tian, J. Gao, S. Yan, Z. Zou, J. Am. Chem. Soc. 132 (2010) 14385–14387.
[20] J. Zhang, F. Guo, X. Wang, Adv. Funct. Mater. 23 (2013) 3008–3014.
[21] X.H. Li, J. Zhang, X. Chen, A. Fischer, A. Thomas, M. Antonietti, X. Wang, Chem. Mater. 23 (2011) 4344–4348.
[22] K. Maeda, X.C. Wang, Y. Nishihara, D. Lu, M. Antonietti, K. Domen, J. Phys. Chem. C 113 (2009) 4940–4947.
[23] Z. Lin, X. Wang, Angew. Chem. Int. Ed. 52 (2013) 1735–1738.
[24] D.J. Martin, K. Qiu, S.A. Shevlin, A.D. Handoko, X. Chen, Z. Guo, J. Tang, Angew. Chem. Int. Ed. 53 (2014) 9240–9245.
[25] Y. Wang, J. Zhang, X. Wang, M. Antonietti, H. Li, Angew. Chem. Int. Ed. 49 (2010) 3356–3359.
[26] H. Zhan, W. Liu, M. Fu, J. Cen, J. Lin, H. Cao, Appl. Catal. A 468 (2013) 184–189.
[27] B. Long, Z. Ding, X. Wang, ChemSusChem 6 (2013) 2074–2078.
[28] X.C. Wang, K. Maeda, A. Thomas, K. Takanabe, G. Xin, J.M. Carlsson, K. Domen, M. Antonietti, Nat. Mater. 8 (2009) 76–80.
[29] J. Lin, Z. Pan, X. Wang, ACS Sustain. Chem. Eng. 2 (2013) 353–358.
[30] G. Dong, L. Zhang, J. Mater. Chem. 22 (2012) 1160–1166.
[31] K. Maeda, R. Kuriki, M. Zhang, X. Wang, O. Ishitani, J. Mater. Chem. A 2 (2014) 15146–15151.

[32] S. Wang, J. Lin, X. Wang, Phys. Chem. Chem. Phys. 16 (2014) 14656–14660.
[33] K. Maeda, K. Sekizawa, O. Ishitani, Chem. Commun. 49 (2013) 10127–10129.
[34] H. Shi, G. Chen, C. Zhang, Z. Zou, ACS Catal. 4 (2014) 3637–3643.
[35] Y.P. Yuan, S.W. Cao, Y.S. Liao, L.S. Yin, C. Xue, Appl. Catal. B 140–141 (2013) 164–168.
[36] S.W. Cao, X.F. Liu, Y.P. Yuan, Z.Y. Zhang, Y.S. Liao, J. Fang, S.C.J. Loo, T.C. Sum, C. Xue, Appl. Catal. B 147 (2014) 940–946.
[37] T. Ohno, N. Murakami, T. Koyanagi, Y. Yang, J. CO_2 Utiliz. 6 (2014) 17–25.
[38] G. Liu, P. Niu, C. Sun, S.C. Smith, Z. Chen, G.Q. Lu, H.-M. Cheng, J. Am. Chem. Soc. 132 (2010) 11642–11648.
[39] P. Niu, L. Zhang, G. Liu, H.-M. Cheng, Adv. Funct. Mater. 22 (2012) 4763–4770.
[40] K. Takanabe, K. Kamata, X. Wang, M. Antonietti, J. Kubota, K. Domen, Phys. Chem. Chem. Phys. 12 (2010) 13020–13025.
[41] Y. Wang, J. Hong, W. Zhang, R. Xu, Catal. Sci. Technol. 3 (2013) 1703–1711.
[42] Y. Zheng, L. Lin, X. Ye, F. Guo, X. Wang, Angew. Chem. Int. Ed. 53 (2014) 11926–11930.
[43] J. Zhang, G. Zhang, X. Chen, S. Lin, L. Möhlmann, G. Dołęga, G. Lipner, M. Antonietti, S. Blechert, X. Wang, Angew. Chem. Int. Ed. 51 (2012) 3183–3187.
[44] J. Zhang, M. Zhang, R.Q. Sun, X. Wang, Angew. Chem. 124 (2012) 10292–10296.
[45] M. Zhang, X. Wang, Ener. Environ. Sci. 7 (2014) 1902–1906.
[46] Y. Chen, J. Zhang, M. Zhang, X. Wang, Chem. Sci. 4 (2013) 3244–3248.
[47] Z. Lin, X. Wang, Chemsuschem 7 (2014) 1547–1550.
[48] J. Liu, T. Zhang, Z. Wang, G. Dawson, W. Chen, J. Mater. Chem. 21 (2011) 14398–14401.
[49] J. Zhang, X. Chen, K. Takanabe, K. Maeda, K. Domen, J.D. Epping, X. Fu, M. Antonietti, X. Wang, Angew. Chem. Int. Ed. 49 (2010) 441–444.
[50] M. Tabbal, T. Christidis, S. Isber, P. Mérel, M.A. El Khakani, M. Chaker, A. Amassian, L. Martinu, J. Appl. Phys. 98 (2005) 44310.
[51] Y. Cui, Z. Ding, X. Fu, X. Wang, Angew. Chem. Int. Ed. 51 (2012) 11814–11818.
[52] S. Soedergren, A. Hagfeldt, J. Olsson, S.E. Lindquist, J. Phys. Chem. 98 (1994) 5552–5556.
[53] M. Kruk, M. Jaroniec, Chem. Mater. 13 (2001) 3169–3183.
[54] Z. Chai, Q. Li, D. Xu, RSC Adv. 4 (2014) 44991–44995.